

Modeling and Prototyping of a Flux Concentrator for Positron Capture

Haitao Wang^{1,2}, Wanming Liu¹, Wei Gai¹, and Thomas Wong²

¹HEP Division, Argonne National Laboratory, Argonne, IL 60439 USA

²ECE Department, Illinois Institute of Technology, Chicago, IL 60616 USA

An adiabatic matching device (AMD) generates a tapered high-strength magnetic field to capture positrons emitted from a positron target to a downstream accelerating structure. The AMD is a key component of a positron source and represents a technical challenge. The International Linear Collider collaboration is proposing to employ a pulsed, normal-conducting, flux-concentrator to generate a 5 Tesla initial magnetic field. The flux-concentrator structure itself and the interactions between the flux-concentrator and the external power supply circuits give rise to a nontrivial system. In this paper, we present a recently developed equivalent circuit model for a flux concentrator, along with the characteristics of a prototype fabricated for validating the model. Using the model, we can obtain the transient response of the pulsed magnetic field and the field profile. Calculations based on the model and the results of measurements made on the prototype are in good agreement.

Index Terms—Equivalent circuit, flux concentrator, mutual inductance, pulsed magnet, transient magnetic field.

I. INTRODUCTION

THE particles emitted from a positron source usually have a broad energy spread and wide angular distribution [1]–[4]. In order to collect the emitted positrons, a matching device is often employed to match the phase space of the positrons to the acceptance aperture of an accelerating structure. The current baseline configuration of the International Linear Collider (ILC) positron source, an adiabatic matching device (AMD), which generates a tapered flux profile with initial magnetic field up to 5 Tesla, is needed for matching the positron beam emerging from the conversion target to the input aperture of the positron pre-accelerator (PPA). Since the AMD will be operating in a radiation-hard environment [5], a pulsed normal conducting flux-concentrator is an optional candidate for fulfilling the requirement [6], [7].

The flux-concentrator first appeared in inductive heating [8]. Applications for producing high intensity pulsed magnetic field were discussed previously [6], [7], [9]–[11]. Fig. 1 shows the cross-sectional views of a typical flux-concentrator. It consists of a primary excitation coil, carrying an azimuthal current, surrounding a solid conducting core with a radial slot running from the inner bore of the core to its outer surface. A time dependent current in the primary coil will induce a magnetic flux in the core. Since there is a slot in the core, an induced current on the outer surface will be directed to flow along the radial direction when it reaches the slot. The direction of the current around the inner contour of the bore will be opposite to that on the outer surface. The induced current generated in the core tends to shift the flux of the primary coil into the smaller region inside the central bore and relieves the mechanical stress arising from the Lorentz force on the primary coil. In addition, a benefit of the flux-concentrator structure is that the field profile can be changed by the shape of the taper.

Due to the complexity of a flux concentrator structure, analytic methods, even approximate ones, are seldom employed in the study of its properties. Numerical methods can be employed

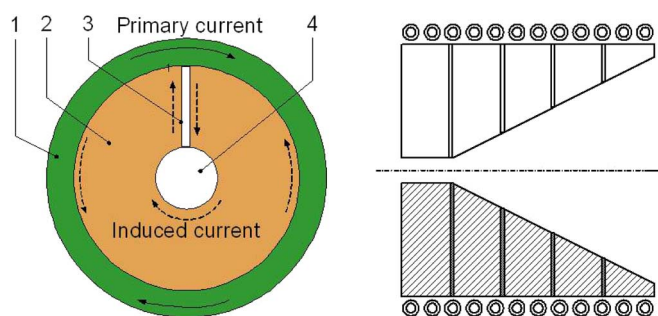


Fig. 1. Cross-sectional views, both longitudinal and transverse, of a typical flux concentrator: 1: primary coil, 2: central core, 3: radial slot, 4: bore.

to obtain the magnetic field as implemented in the studies of magnetic devices, for which a coupling of the field solution to the external circuits has been developed [12], [13], [17]. In this investigation, an alternative approach to modeling the magnetic device is employed. It is based on coupled distributed circuits consisting of self and mutual inductance and resistance for both the core region and the coil. In this way, the interface with external circuit is readily accessible at the terminals of the coil, while the core region is partitioned into a sequence of coupled two-dimensional structures, each modeled by distributed equivalent circuits. The formulation is distributed in nature and has been successfully applied to calculate the skin effect in transmission lines [14], [15]. Interface with external driver circuit can be incorporated in an efficient manner.

In order to verify the effectiveness of this model, a prototype flux-concentrator was designed and built. Result of measurements of the prototype at room temperature is compared to the prediction by the model and the observations are discussed in this paper.

II. EQUIVALENT CIRCUIT MODEL

A. Modeling of Flux Concentrator With Partitions

Modeling of the flux concentrator begins with dividing the central core into thin axial disks along the axial direction, followed by subdividing each disk into concentric rings, as shown in Fig. 2. Adjacent rings are connected with each other at the slot location. Let the disks be numbered from 1 to G. Each disk will have a different number of rings due to the tapered section.

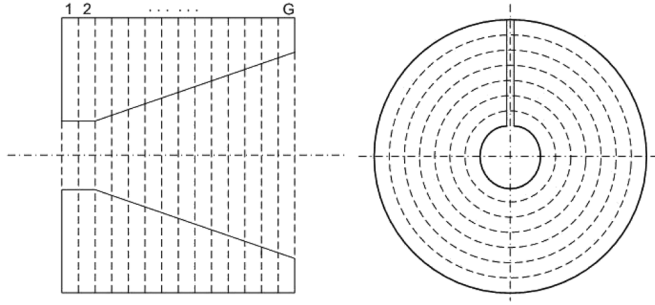


Fig. 2. Partitioning of a flux concentrator.

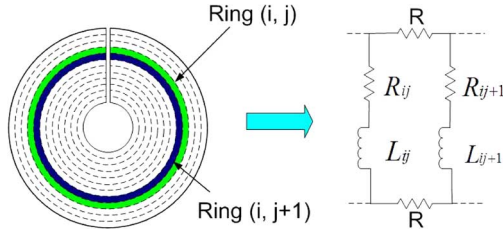


Fig. 3. Two adjacent rings within the same disk form a circuit loop.

The i th disk has N_i concentric rings. The rings will be labeled as (i, j) , which is referred to as the j th ring of the i th disk. There are N_{tot} concentric rings, where

$$N_{\text{tot}} = \sum_{i=1}^G N_i. \quad (1)$$

The accuracy of the model will depend on the meshing process, as reflected by the number of disks G . The final number was determined by gradually increasing G until the parameters obtained by the model settled within 0.1%. This occurred when the thickness of the disks was limited to 2 mm for the prototype structure to be described in the following sections.

We assume the current in a concentric ring flows azimuthally, without crossing the boundaries of the ring, except when interconnecting with other rings within the same axial disk at the slot location. We justify this assumption by noting that the magnetic field inside the core only has radial and axial components, except at the slot area. In addition, we assume that the current density within each ring is uniform but varying from ring to ring. With these assumptions, the concentric rings are modeled using lumped circuit parameters.

Each concentric ring is modeled as a circuit branch, including a resistor R_{ij} and an inductor L_{ij} that are serially connected together. To model the slot effect, we introduce an equivalent resistor, R , which is frequency dependent. This approximation simplifies the circuit model from 3-D to 2-D, and greatly reduces the computation time. Any two adjacent rings within the same disks are connected by two equivalent resistors at the slot location to form a circuit loop. Fig. 3 shows a circuit loop formed by rings (i, j) and $(i, j+1)$. R is the equivalent resistor connecting the two rings at the slot location.

We can also model the primary coil as a resistor R_p and an inductor L_p that are serially connected, with mutual inductances accounting for its coupling to the rings in the core, to be described in Figs. 4 and 5. Since there is always loss in a practical power supply, and the cables connecting the power source with

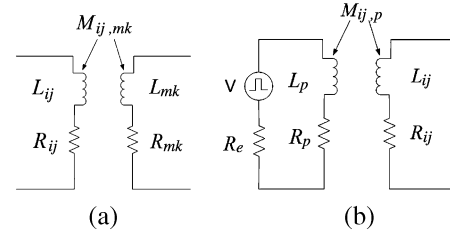
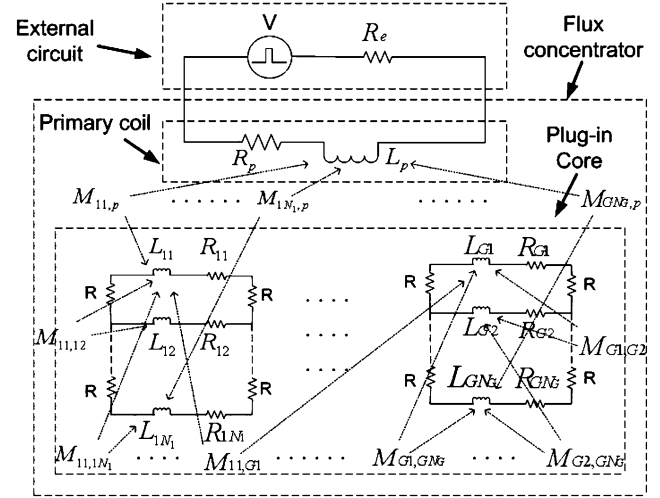
Fig. 4. Modeling of coupling in a flux concentrator, (a) coupling between two concentric rings (i, j) and (m, k) , (b) coupling between the primary coil and ring (i, j) .

Fig. 5. Modeling of the entire flux concentrator including primary coil and external circuit.

the primary coil also introduce some loss, the external circuit is modeled as an ideal voltage source, V , serially connected with a small external resistor, R_e . The coupling between rings and rings to the primary coil are mediated by mutual inductance, M . Fig. 4(a) shows the coupling between any two rings (i, j) and (m, k) . The coupling between the primary coil and ring (i, j) is illustrated in Fig. 4(b). Finally, we model the entire flux concentrator with the external power supply circuit as shown in Fig. 5.

B. Calculation of Circuit Parameters

With the assumptions mentioned in the previous section, the DC resistance R_{ij} for the concentric ring (i, j) is calculated as

$$R_{ij} = \frac{\rho l_{ij}}{A_{ij}} \quad (2)$$

where ρ is the resistivity of the central core, l_{ij} is the length of the concentric ring (i, j) , and A_{ij} is the cross-sectional area of the ring.

The equivalent resistance, R , connecting two adjacent rings at the slot location is calculated as

$$R = \frac{\rho d}{w \delta} \quad (3)$$

where d is the distance between the centers of two adjacent rings, w is the ring width along the axial direction, and δ is the skin depth, which is expressed as

$$\delta = \sqrt{\frac{\rho}{\pi\mu f}} \quad (4)$$

where μ is the permeability of the core material, and f is the frequency.

Using Neumann's formula [16], [], the mutual inductance between two concentric rings, with radius r_1 and r_2 , and distance d between their centers, can be calculated as

$$M = \frac{\mu_0}{4\pi} \int_0^{2\pi} \int_0^{2\pi} \frac{r_1 r_2 \cos(\varphi - \varphi') d\varphi d\varphi'}{\sqrt{r_1^2 + r_2^2 + d^2 - 2r_1 r_2 \cos(\varphi - \varphi')}}. \quad (5)$$

The integral from (5) can be exactly solved analytically as

$$M = -\mu_0 \sqrt{r_1 r_2} \left[\left(k - \frac{2}{k} \right) K + \frac{2}{k} E \right] \quad (6)$$

where the modulus k is

$$k = \frac{2\sqrt{r_1 r_2}}{\sqrt{(r_1 + r_2)^2 + d^2}}.$$

K and E are the complete elliptic integrals of first and second kinds

$$K = \int_0^{\frac{\pi}{2}} \frac{d\varphi}{\sqrt{1 - k^2 \sin^2 \varphi}}$$

$$E = \int_0^{\frac{\pi}{2}} \sqrt{1 - k^2 \sin^2 \varphi} d\varphi. \quad (7)$$

Due to the existence of the slot, the rings are not closed. Hence, the inductance calculation by (6) needs to be modified to include this effect. We assumed that the mutual inductance of the full ring ((6)) is reduced by $\theta/2\pi$, therefore the following is the modified equation:

$$M = -\frac{\mu_0 \theta_1 \theta_2 \sqrt{r_1 r_2}}{4\pi^2} \left[\left(k - \frac{2}{k} \right) K + \frac{2}{k} E \right]. \quad (8)$$

Here, θ_1 and θ_2 are angles of two partial rings.

Similarly, we can calculate the resistance and inductance of the primary coil. The mutual inductance $M_{ij,p}$ between the coil and ring (i, j) is calculated as follows:

$$M_{ij,p} = \sum_{m=1}^{N_c} -\frac{\mu_0 \theta_{ij} \sqrt{r_{ij} r_m}}{2\pi} \left[\left(k - \frac{2}{k} \right) K + \frac{2}{k} E \right] \quad (9)$$

where θ_{ij} is the angle of partial ring (i, j) , r_{ij} is the radius of ring (i, j) , N_c is number of turns of the primary coil, and r_m is the radius of turn m , here $m = 1, 2, \dots, N_c$. While the coupling coefficient between the coil and the core is not expected to be high since no ferromagnetic or high permeability material was employed, no attempt was made to estimate the coefficient. The mutual inductances were obtained directly from (6) and (9).

C. Coupled Circuit Equations

The upper part in Fig. 5 is the primary loop, which includes voltage source, V , equivalent external resistance, R_e , resistance and inductance of the primary coil, R_p and L_p , and the coupling from the central core, $M_{ij,p}$. According to Kirchhoff's Voltage Law, with the assumption that the currents in the primary coil and concentric rings have the same direction, the circuit equation in the primary loop in frequency domain can be expressed as

$$v = R_e i_p + (R_p + j\omega L_p) i_p + \sum_{i=1}^G \sum_{j=1}^{N_i} j\omega M_{ij,p} i_{ij} \quad (10)$$

where v is the externally applied voltage from the source, i_p is the current in the primary coil, i_{ij} is the current flowing through ring (i, j) , ω is the angular frequency, and j is the square root of -1 .

As mentioned earlier, the i th disk consists of N_i rings. Any two adjacent rings form a circuit loop. Hence, there are $N_i - 1$ independent circuit loops totally for disk i . For the circuit loop formed by ring (i, j) , ring $(i, j + 1)$, and the slot equivalent resistor, R , the circuit equation can be expressed as

$$j\omega M_{ij,p} i_p + (R_{ij} + j\omega L_{ij}) i_{ij} + \sum_{m_1=1}^G \sum_{k_1=1}^{N_{m_1}} j\omega M_{ij,m_1 k_1} i_{m_1 k_1} \delta_{m_1 k_1} + 2R \sum_{k=1}^j i_{ik} - j\omega M_{i(j+1),p} i_p - (R_{i(j+1)} + j\omega L_{i(j+1)}) i_{i(j+1)} - \sum_{m_2=1}^G \sum_{k_2=1}^{N_{m_2}} j\omega M_{i(j+1),m_2 k_2} i_{m_2 k_2} \delta_{m_2 k_2} = 0 \quad (11)$$

where

$$\begin{cases} \delta_{m_1 k_1} = 0 & \text{if } m_1 = i \text{ and } k_1 = j, \\ \delta_{m_1 k_1} = 1 & \text{Otherwise} \end{cases}$$

and

$$\begin{cases} \delta_{m_2 k_2} = 0 & \text{if } m_2 = i \text{ and } k_2 = j + 1, \\ \delta_{m_2 k_2} = 1 & \text{Otherwise.} \end{cases}$$

According to Kirchhoff's Current Law, the following equation is obtained for disk i , ($i = 1, 2, \dots, G$) from Fig. 5:

$$\sum_{j=1}^{N_i} i_{ij} = 0. \quad (12)$$

Hence, from (10)–(12), a total of $N_{\text{tot}} + 1$ equations are arrived at. Finally, we express the coupled circuit system with matrix format as

$$Z \times I = V. \quad (13)$$

Here,

$$\begin{aligned}
 I & [i_p, i_1, i_2, \dots, i_{N_{\text{tot}}}]', \\
 V & [v, 0, 0, \dots, 0]', \\
 Z & (N_{\text{tot}} + 1) \times (N_{\text{tot}} + 1) \text{ matrix of circuit parameters.}
 \end{aligned}$$

By solving the systems of equations, the frequency domain solutions of the currents in the primary coil and all the concentric rings can be obtained.

D. Calculation of Magnetic Field

From the solution of the frequency domain current distribution, the calculation of magnetic flux density at a reference location of the central axis for any single concentric ring (i, j) is straightforward with a given current using the following equation:

$$B_{zij} = \frac{\mu_0}{2} \frac{r_{ij}^2 i_{ij}}{(r_{ij}^2 + z_{ij}^2)^{3/2}} \quad (14)$$

where B_{zij} is the on-axis magnetic flux density at the reference plane, i_{ij} is the current flowing through the concentric ring (i, j) , μ_0 is permeability of air, r_{ij} is the radius of the ring, and z_{ij} is the relative position of the ring to the reference plane along axial direction.

For the calculation of B_{zij} in the flux-concentrator, we make the assumption that the ring is not a partial but complete circle, so that in employing (14) for the calculation of the magnetic field, the effect of the slot is neglected. This is justified by noting that while the presence of the slot is vital for interrupting the azimuthal current and redirecting it to eventually flow in an opposite sense in the inner core, the slot itself makes little contribution to the total magnetic flux in the bore, since the currents on the two walls facing the slot gap are opposite to each other and tend to cancel when the slot is narrow. The apparent approximation in neglecting the slot is therefore only in the extra ampere-turn due to the gap region incorporated in (14). A numerical calculation by summing the contributions across the slot gap gave an error of less than 3% in the total flux density along the axis of the bore. By incorporating the effects from all the current rings of the flux concentrator and the primary coil, the frequency domain solution of magnetic field at any given point is obtained and the transient response of the magnetic field can be found by performing inverse Fourier Transform. By varying the longitudinal position of the reference plane, the distribution of on-axis magnetic field can be calculated in the same way.

III. DEVELOPMENT OF PROTOTYPE

A. Experimental System

In order to assess the validity of the circuit model, a prototype flux-concentrator was assembled using a coil formed from copper tubing and a plug-in aluminum core. Fig. 6 shows the cross section and a picture of the prototype. The excitation coil has 168 turns, wound with rectangular copper tubing, 0.64 cm \times 0.64 cm in cross section. The plug-in core, 24 cm in diameter and 8.7 cm in length, is made of aluminum. A bore is cut inside the core. The bore starts with a straight section, followed by a 45° tapered section. The straight section has a diameter of 2 cm.

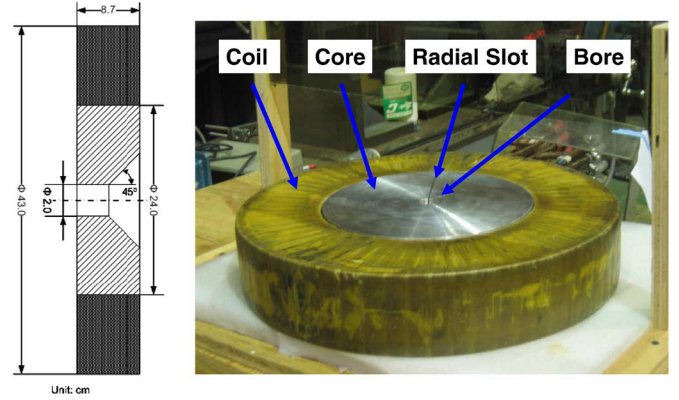


Fig. 6. Cross section and picture of a prototype flux concentrator, which includes a coil surrounding an aluminum core.

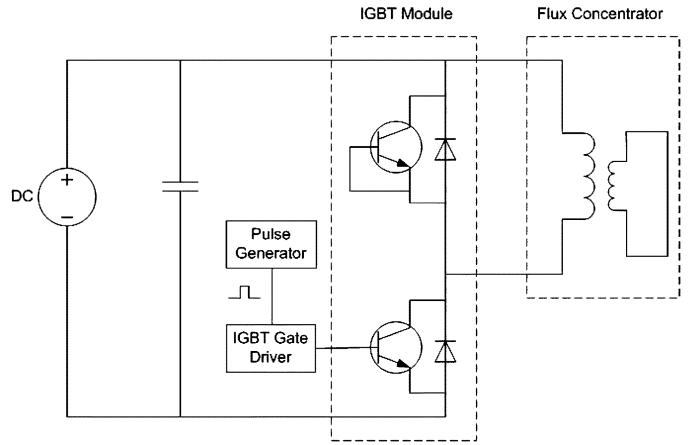


Fig. 7. Experiment system setup of a prototype flux concentrator.

As an important part of the prototype system, a pulsed power supply was designed by integrating an insulated-gate bipolar transistor (IGBT) module, Powerex CM200DY-12NF, with a regulated dc power supply. The entire experimental circuit of the prototype flux concentrator is shown in Fig. 7. The IGBT module includes two transistors with free-wheeling diodes. The gate and emitter terminals of the upper transistor are shorted, and the lower transistor is connected to the IGBT gate driver. When a pulse signal from the pulse generator enters the IGBT gate driver, a control voltage from the gate driver is applied across the gate and emitter terminals of the lower transistor to drive the switch on or off.

B. Measurements of Transient Responses

With the experimental system in place, the prototype flux-concentrator was experimentally characterized at room temperature. To gain insight into the operational mechanism of a flux-concentrator, we made measurements on three configurations. The first one is referred to as *coil-only configuration*, which solely consists of the excitation coil without the plug-in aluminum core; the second one is the *no-slot configuration*, which includes the excitation coil and the plug-in core but no radial slot is cut; and the last one is the *flux-concentrator*, which includes the coil and the plug-in core with slot. For all three configurations we measured the transient response of the voltage across the coil terminals, the current flowing through the coil,

and the axial magnetic flux density, B_z , on the central axis of the coil assembly. The pulsed current was measured by using a current probe, LEM PR 430, which is based on Hall effect with frequency range from dc to 20 kHz. The pulsed magnetic field was measured by using a Hall effect magnetic sensor, Honeywell SS495A1. The magnetic sensor was calibrated prior to measurement. All the measured data were displayed by an oscilloscope, Tektronix TDS540, and read out to a computer using a GPIB adapter.

Fig. 8 shows the transient responses of the voltage, current, and axial magnetic flux density, B_z , for the three configurations excited with a voltage pulse of 50 ms pulsewidth from the pulsed power source. Fig. 8(a) shows the measured results for the coil-only configuration, Fig. 8(b) is for the no-slot configuration, and Fig. 8(c) is for the flux-concentrator. The voltage and current curves show very little difference for the three configurations. The rising edge of the voltage is around 3.3 V, followed by a gradual reduction with the increase in current in the coil. The transient current curves have a peak current of around 11 A, although there is a small difference in the time constant. The difference in the curves of the transient magnetic flux density is very remarkable, as expected.

For the *coil-only configuration*, the transient magnetic flux density increases gradually and reaches the peak at the pulse's falling edge (time = 50 ms). The transient magnetic flux density for the *no-slot configuration* increases very slowly in the rising period of the exciting pulse, and reaches the peak after the falling edge of the exciting voltage pulse, reflecting that the induced current in the plug-in core is to counteract the change of the current in the coil. The transient magnetic flux density of the *flux-concentrator* rises more quickly and the peak magnetic flux density shows a more than 30% gain over that of the coil-only configuration. The field enhancement comes from the fact that the induced current in the core tends to shift the flux generated by the primary coil into the smaller region inside the central bore. A detailed analysis is presented in the following section.

C. Measurements of Field Profiles

To study the effect of the bore shape on magnetic field profile, a half tapered and half straight bore was machined in the plug-in core. The axial transient magnetic flux densities, B_z , were measured along the central axis, Z , for both the no-slot configuration and flux concentrator. Both field profiles were plotted at the falling edge of the exciting voltage pulse ($t = 50$ ms) as shown in Fig. 9. $Z = 0$ cm shows the starting position of the central core. For the flux concentrator, the peak axial magnetic flux density is located near the joint of the tapered and straight sections. The field decreases gradually on the side of the tapered section. On the side of the straight section, the field first reduces slightly, and shows a rapid drop after leaving the straight section ($Z = 0$ cm). For the no-slot configuration the axial magnetic flux density forms a valley near the joint, with peaks outside the end surfaces of the central core on both sides.

IV. COMPARISON WITH RESULTS FROM MODEL

Employing the distributed circuit model developed in the previous section, transient currents and magnetic flux densities were calculated for the no-slot configuration and the flux concentrator with same geometry and materials. Fig. 10 shows the

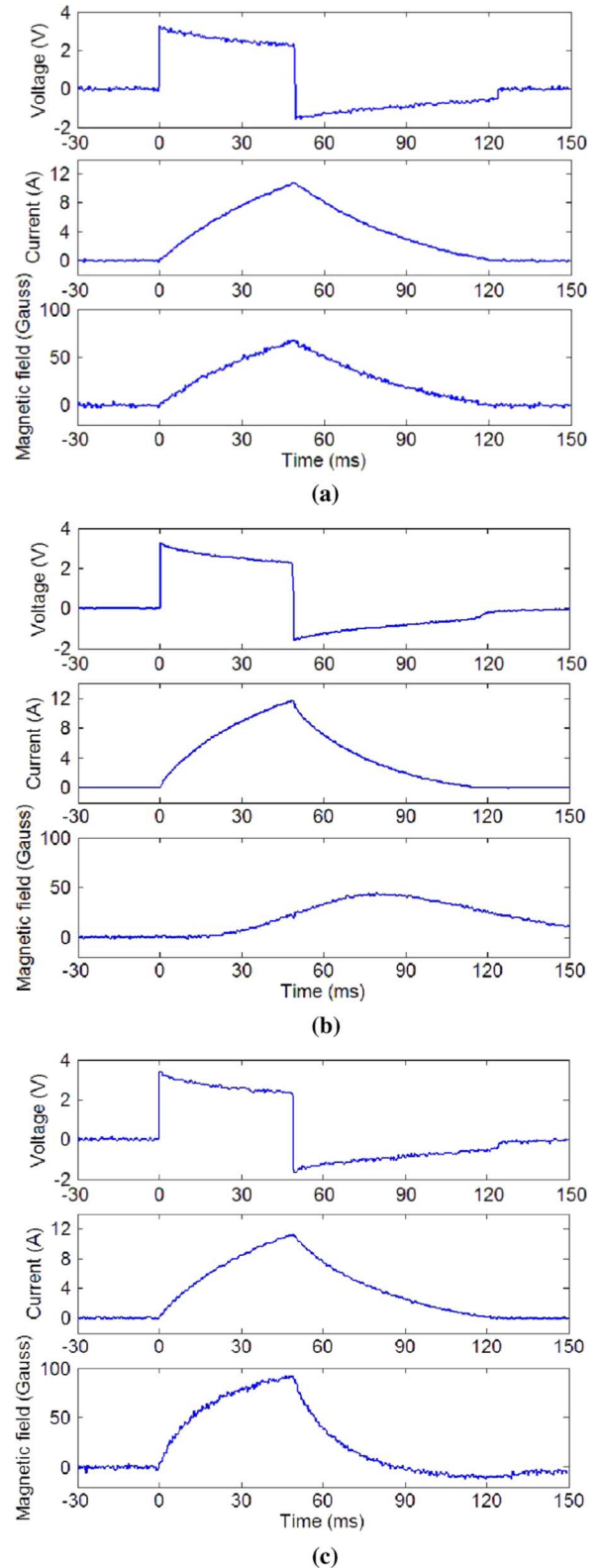


Fig. 8. Transient responses of the voltage, current and axial magnetic flux density, B_z , for three configurations: (a) coil only configuration, (b) no-slot configuration, and (c) flux concentrator.

distribution of typical induced currents in the plug-in core for the no-slot configuration. For a given disk, we plot the transient current for three different rings of the plug-in core. The ring currents have the same direction, but opposite to that in the

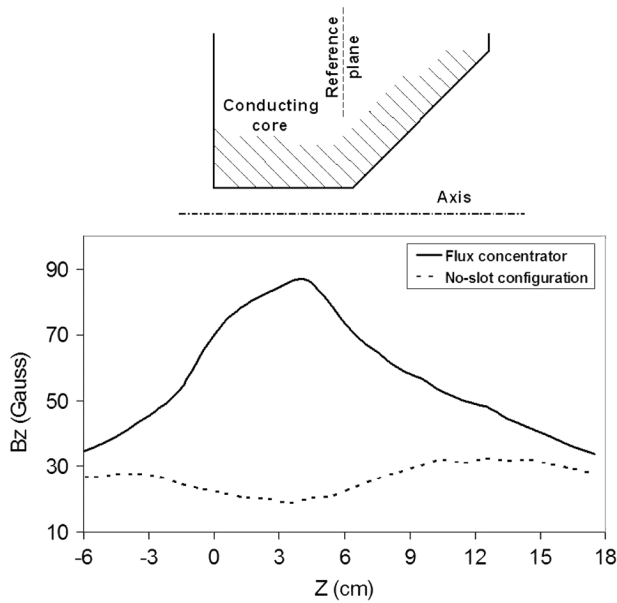


Fig. 9. Measured field profiles along the central axis at time instant 50 ms for both flux concentrator and no-slot configuration. The starting position of the plug-in core is located at $Z = 0$ cm.

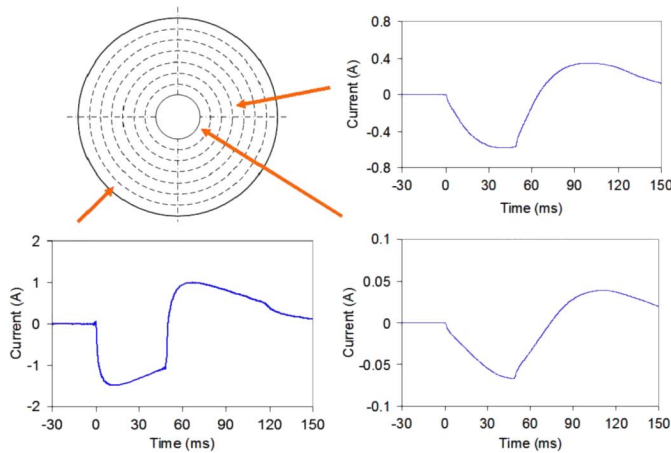


Fig. 10. The typical current distribution in the plug-in core for the no-slot configuration.

coil. The amplitude of the currents varies dramatically along the radial direction. The peak current on the outer surface is much larger than that on the inner surface. The induced current in the core counteracts the magnetic field produced by the coil, and causes the transient magnetic field curve to slowly increase during the rising section of the current waveform, eventually form peak at the falling section of the current waveform, as shown in Fig. 8(b). The typical transient current curves in the plug-in core of the flux concentrator are shown in Fig. 11. The current on the bore surface has almost the same magnitude as that on the outer surface of the core, but their directions are opposite. The direction of the current on the bore surface is the same as that in the coil. Compared with the currents on the surfaces, the currents at the interior of the core are much smaller in magnitude. These phenomena agree well with the operational mechanism of a flux concentrator.

Based on the calculation of currents in the coil and plug-in core, we can obtain the transient magnetic field curves in the

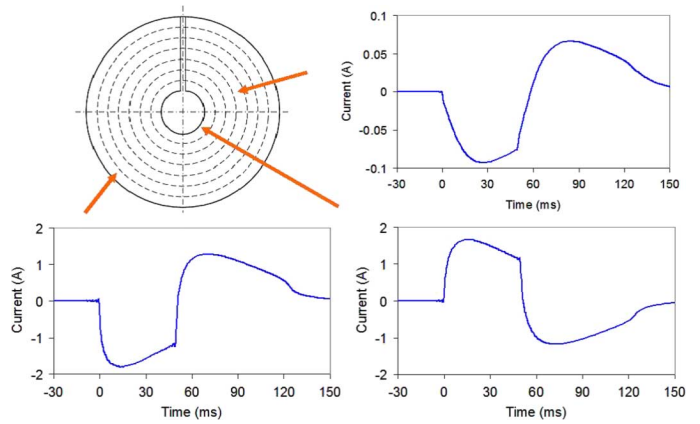


Fig. 11. The typical current distribution in the plug-in core of the prototype flux concentrator.

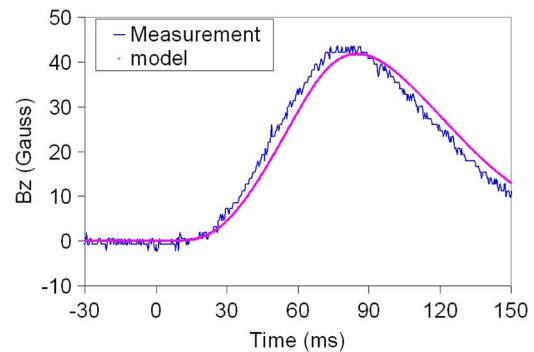


Fig. 12. Comparison of the measured magnetic field with the modeling results for the no-slot configuration.

middle of the central axis for both the no-slot configuration and the flux concentrator. Fig. 12 shows the comparison of the measured transient axial magnetic flux density, B_z , with the modeling results for the no-slot configuration. The comparison of the transient magnetic flux density for the flux concentrator is shown in Fig. 13. For both configurations, we also calculated the transient axial magnetic flux densities, B_z , at different locations along the central axis, Z , using the circuit model, and obtained the field profiles at the falling edge of the exciting voltage pulse (time = 50 ms). Fig. 14 shows the comparison of the measured field profile with the simulated results for no-slot configuration. The comparison of the field profiles for the flux concentrator is shown in Fig. 15.

From the comparisons, one observes that the predictions by the circuit model exhibit good agreement with the measured data. The small difference between the measured data and the calculation is ascribed to an overestimation on the coupling between the plug-in core and the primary coil and an underestimation in the core losses.

V. CONCLUSION

A distributed circuit model has been proposed for calculating the transient response of a flux-concentrator. To validate the model a prototype flux-concentrator was designed and built. Three configurations were excited by a current pulse and their transient responses measured: coil-only configuration, no-slot configuration, and flux-concentrator configuration. The measurements showed that compared to that of the coil-only

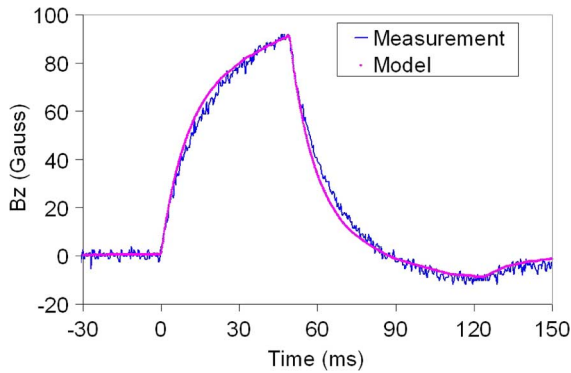


Fig. 13. Comparison of the measured magnetic field with the modeling results for the flux concentrator.

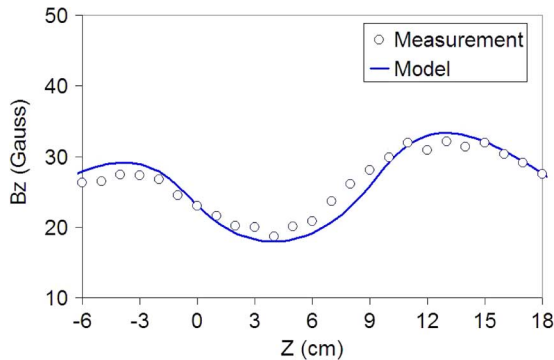


Fig. 14. Comparison of the measured on-axis field profile with the modeling results for the no-slot configuration.

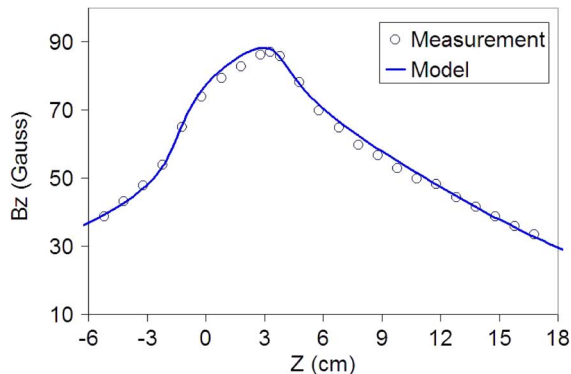


Fig. 15. Comparison of the measured on-axis field profile with the modeling results for the flux concentrator.

configuration the peak magnetic field of the flux-concentrator increased by more than 30%, whereas for the no-slot structure the peak magnetic field decreased by approximately more than 40%.

Magnetic field profiles for both the no-slot configuration and flux-concentrator with half tapered and half straight bore shape were measured. The measured data accurately matched the variation of the field profile in both the tapered and straight sections.

The transient current distribution in the plug-in core and the transient magnetic fields were calculated using the respective circuit models for the no-slot configuration and the flux-concentrator. The induced current distribution in the core evidently accounts for the enhancement effect on the magnetic field of the flux-concentrator and the field characteristics of the no-slot configuration. The transient magnetic fields and field profiles calculated by the circuit model for both the no-slot configura-

tion and the flux-concentrator showed good agreement with the measured data.

ACKNOWLEDGMENT

This work was supported by the U.S. Department of Energy Office of Science under Contract DE-AC02-06CH11357, and conducted at High Energy Physics Division of Argonne National Laboratory. The authors gratefully acknowledge their support.

REFERENCES

- [1] K. Flottmann, "Investigations Towards the Development of Polarized and Unpolarized High Intensity Positron Sources for Linear Colliders," Ph.D. dissertation, Univ. Hamburg, Hamburg, Germany, 1993, DESY 93-161.
- [2] V. Bharadwaj, Y. Batygin, R. Pitthan, J. Sheppard, H. Vincke, J. W. Wang, J. Gronberg, and W. Stein, "Design issues for the ILC positron source," in *Proc. Particle Accelerator Conf.*, Knoxville, TN, 2005, pp. 3230–3232.
- [3] W. Liu, W. Gai, and K.-J. Kim, "Systematic study of undulator based ILC positron source: Production and capture," presented at the *Proc. Particle Accelerator Conf.*, Albuquerque, 2007, THPMN090.
- [4] T. Omori, T. Aoki, K. Dobashi, T. Hirose, Y. Kurihara, T. Okugi, I. Sakai, A. Tsunemi, J. Urakawa, M. Washio, and K. Yokoya, "Design of a polarized positron source for linear colliders," *NIMA*, vol. 500, pp. 232–252, Mar. 2003.
- [5] A. Ushakov, E. Elsen, K. Flottmann, S. Riemann, and K. Sanisyan, "Radiation levels and activation at the ILC positron source," in *Proc. EPAC 2006*, Edinburgh, Scotland, pp. 2478–2480.
- [6] A. V. Kulikov, S. D. Ecklund, and E. M. Reuter, "SLC positron source pulsed flux concentrator," in *Proc. Particle Accelerator Conf.*, San Francisco, CA, 1991, pp. 2005–2006, SLAC-PUB-5473.
- [7] G. Stange, "A small size 7 Tesla flux-concentrator of modular construction fed by a small thyristor pulse generator," *IEEE Trans. Magn.*, vol. MAG-20, no. 5, pp. 1810–1812, Sep. 1984.
- [8] G. Babat and M. Losinsky, *J. Appl. Phys.*, vol. 11, p. 816, 1940.
- [9] H. Brechna, D. A. Hill, and B. M. Bally, "150 kOe liquid nitrogen cooled pulsed flux-concentrator magnet," *Rev. Sci. Instrum.*, vol. 36, pp. 1529–1535, Nov. 1965.
- [10] Y. B. Kim and E. D. Platner, "Flux concentrator for high-intensity pulsed magnetic fields," *Rev. Sci. Instrum.*, vol. 30, pp. 524–533, Jul. 1959.
- [11] M. N. Wilson and K. D. Srivastava, "Design of efficient flux concentrators for pulsed high magnetic fields," *Rev. Sci. Instrum.*, vol. 36, pp. 1096–1100, Aug. 1965.
- [12] P. J. Leonard, R. J. Hill-Cottingham, and D. Rodger, "3D finite element models and external circuits using the $A\psi$ scheme with cuts," *IEEE Trans. Magn.*, vol. 30, no. 5, pp. 3220–3223, Sep. 1994.
- [13] A. Nicolet, F. Delince, N. Bamps, A. Genon, and W. Legros, "A coupling between electric circuits and 2D magnetic field modeling," *IEEE Trans. Magn.*, vol. 29, no. 2, pp. 1697–1700, Mar. 1993.
- [14] T. Vu Dinh, B. Cabon, and J. Chilo, "New skin-effect equivalent circuit," *Electron. Lett.*, vol. 26, no. 19, pp. 1582–1584, Jul. 1990.
- [15] W. T. Weeks, L. L. Wu, M. F. McAllister, and A. Singh, "Resistive and inductive skin effect in rectangular conductor," *IBM J. Res. Develop.*, vol. 23, no. 6, Nov. 1979.
- [16] S. Ramo, J. R. Whinnery, and T. V. Duzer, *Fields and Waves in Communication Electronics*. New York: Wiley, 1965, pp. 306–308.
- [17] V. Thiagarajan and K. Hsieh, "An algorithm to couple an external RL circuit with the finite-element code EMAP3D," *IEEE Trans. Magn.*, vol. 43, no. 1, pp. 376–379, Jan. 2007.
- [18] S. I. Babic and C. Akyel, "New analytic-numerical solutions for the mutual inductance of two coaxial circular coils with rectangular cross section in air," *IEEE Trans. Magn.*, vol. 42, no. 6, pp. 1661–1669, Jun. 2006.